JOURNAL OF SOLID STATE CHEMISTRY **121,** 423–429 (1996)
ARTICLE NO. 0058

Crystal Structure and Metal–Insulator Transition of $La_{1-x}Sr_xCoO_3$

Atsushi Mineshige, Minoru Inaba,[1] Takeshi Yao, and Zempachi Ogumi

Division of Energy and Hydrocarbon Chemistry, Graduate School of Engineering, Kyoto University, Sakyo-ku, Kyoto 606-01, Japan

Kenji Kikuchi

Department of Materials Science, University of Shiga Prefecture, Hikone, Shiga 522, Japan

and

Masaya Kawase

Department of Chemistry, Faculty of Education, Kagawa University, Takamatsu, Kagawa 760, Japan

Received March 13, 1995; in revised form August 22, 1995; accepted October 23, 1995

Crystal structure of perovskite $La_{1-x}Sr_xCoO_3$ ($0.0 \leq x \leq 0.7$) was precisely determined by powder X-ray Rietveld analysis, and its correlation with the electrical properties was discussed. The space group was assigned to rhombohedral $R\bar{3}c$ in the range $0.0 \leq x \leq 0.5$ and to cubic $Pm3m$ in the range $0.55 \leq x \leq 0.7$. At $x \sim 0.25$ the Co–O distance and Co–O–Co angle of this system showed an abrupt decrease and increase with increasing x, respectively, and the conductivity behavior changed from semiconducting to metallic. The abrupt changes in crystal structure were attributed to a change in the band structure at the transition from semiconducting to metallic, that is, an increase in the overlap between the valence band and doped hole sates.

1. INTRODUCTION

Doped lanthanum cobaltite, in particular, strontium-doped $La_{1-x}Sr_xCoO_3$ has high electrical and ionic (O^{2-}) conductivities, and hence is a promising material for use as a cathode in solid oxide fuel cells (1, 2) and for oxygen permeation membranes (3). The crystal structure, and electrical and magnetic properties of undoped and Sr-doped lanthanum cobaltite have been studied for several decades (4–12). Furthermore, $La_{1-x}Sr_xCoO_3$ has recently attracted much attention of many workers because it exhibits metal–insulator (M–I) transition by Sr-doping or temperature rise (13–17).

Although many workers have stressed that the metal–oxygen distance and the metal–oxygen–metal angle play an important role in the electrical conduction of transition-metal compounds, there have been few precise crystallographic studies for $La_{1-x}Sr_xCoO_3$, in particular, on the variation with Sr-doping. In order to understand the origin of the M–I transition, it is important to clarify the correlation between the crystal structure and electric conductivity. In the present work, we precisely determined the lattice parameters and interatomic distances and angles of $La_{1-x}Sr_xCoO_3$ using the powder X-ray Rietveld method. The correlation of the changes in crystallographic parameters with the electrical properties was also discussed.

2. EXPERIMENTAL

$La_{1-x}Sr_xCoO_3$ samples were prepared by a conventional solid phase reaction. Mixtures of La_2O_3, $CoCO_3$, and $SrCO_3$ powders in the desired ratios ($0.0 \leq x \leq 0.7$) were pressed into pellets. Two kinds of firing patterns were used in this study. In the first pattern, the pellets were fired at 1473 K for 12 h in air, and cooled at ca. 600 K/h to room temperature (fast-cooled samples). This process was repeated, usually three times, until each lattice constant of the perovskite converged within 0.1% in relative difference. In the second pattern, the pellets of the mixtures were fired at 1473 K for 5 h in air, annealed at 1273 K for 12 h, and then cooled to room temperature at 42 K/h (slowly cooled samples). These fired samples were ground for 2 h prior to X-ray diffraction measurements. A perovskite single phase was obtained for each sample.

X-ray diffraction patterns were obtained at room temperature using a Rigaku RAD-B system. Mo$K\alpha$ radiation was used as an X-ray source in order to avoid the dispersive and absorption effects of Cu$K\alpha$ radiation on Co atoms. The accelerating voltage and current were 45 kV and 40

[1] To whom correspondence should be addressed.

0022-4596/96 $18.00

mA, respectively. To obtain diffraction patterns, 2θ angle was step-scanned from 10° to 60° with a step width of 0.01° and an integration time of 15 s. The crystal structures of the samples were refined using a powder X-ray Rietveld program RIEVEC (18–22). Rhombohedral $R\bar{3}c$ was used as a space group for Rietveld refinements for samples in the range $0.0 \leq x \leq 0.5$ (8), and cubic $Pm3m$ was used in the range $0.55 \leq x \leq 0.7$. Interatomic distances and angles were calculated from the oxygen coordinates obtained by the Rietveld method.

The ratio of the cations of each sample was determined by inductively coupled plasma spectrometry (ICP), and the mean valence of cobalt by iodometry (4).

The pellets of fast-cooled samples were cut into bars and used for electric conductivity measurements. The conductivity was measured from room temperature to 1473 K in air by a standard d.c. four-probe method (9, 12). To minimize joule heating (12), a small current was applied so that the potential difference between the inner two probes was maintained less than 5 mV. The relative density of each sample was higher than 85%.

3. RESULTS AND DISCUSSION

3.1 Nonstoichiometry

The cation ratio of each sample determined by ICP was almost in agreement with that of the starting mixture. Mean valences of cobalt (n) determined by iodometry are plotted against Sr content (x) in Fig. 1. While the values were close to the stoichiometric ones and an approximately linear relationship with x was observed at $x < 0.55$, the deviation from the stoichiometry became significant at $x > 0.55$. The excess charge induced by Sr-doping to $LaCoO_3$ is compensated by the creation of holes, that is, the oxidation of Co^{3+} to Co^{4+}, or by the creation of oxygen vacancies. The deviation from the stoichiometry means the presence of oxygen vacancies. Jonker and Van Stanten (4) studied the oxygen nonstoichiometry of $La_{1-x}Sr_xCoO_3$ prepared in an oxygen atmosphere and reported that the oxidation of Co^{3+} ions was preferable to the creation of oxygen vacancies at $x < 0.5$, while the creation of oxygen vacancies was predominant at $x > 0.5$. A similar tendency was observed in this study; however, the presence of oxygen vacancies was recognized even at $x < 0.5$ in our samples, although the amount was small. The samples should therefore be described as $La_{1-x}Sr_xCoO_{3-\delta}$. The δ values were 0.01 (x = 0.0), 0.02 (x = 0.1), 0.04 (x = 0.3), 0.08 (x = 0.5), and 0.16 (x = 0.7) for fast-cooled samples, respectively.

We used two firing patterns for sample preparation, aiming to change the concentration of oxygen vacancies in the samples. However, the cooling rate sparingly affected the concentration of oxygen vacancies. It is known that the diffusion coefficient of oxygen vacancy in $La_{1-x}Sr_xCoO_3$ is very large ($D_v \sim 10^{-5}$ cm^2/s at 1273 K) (23). Hence, the oxygen vacancy of the samples may have been nearly in equilibrium with the atmosphere even during fast-cooling, or equilibrium may have been attained during grinding.

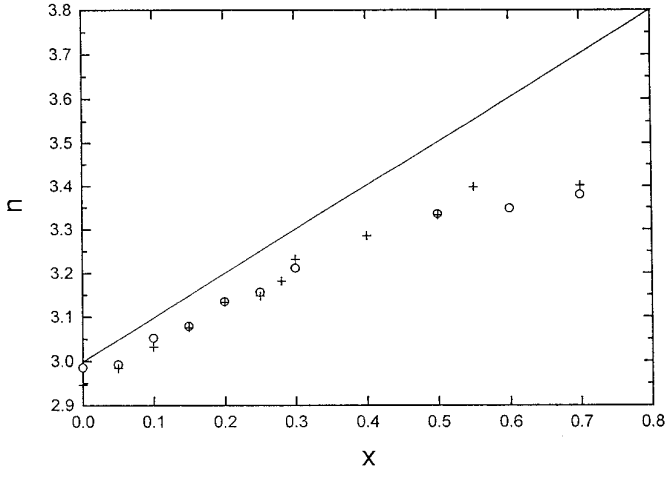

FIG. 1. Relation between mean valence of cobalt n and x in $La_{1-x}Sr_xCoO_3$ samples; (○) cooled at ca. 873 K/h, and (+) annealed at 1273 K for 12 h and cooled at 42 K/h. The solid line shows a theoretical curve for stoichiometric compositions.

3.2 Lattice Parameters, and Interatomic Distances and Angles

Figure 2 shows representative experimental and calculated XRD profiles for the fast-cooled $La_{0.7}Sr_{0.3}CoO_3$ sample (R_{wp} = 7.7%). The Rietveld profile refinement gave precise fitting for each sample with a reliability factor (R_{wp}) less than 8%. The crystal structure of $La_{1-x}Sr_xCoO_3$ is shown in Fig. 3 and the lattice parameters refined by the Rietveld method are shown in Fig. 4, where a_h and c_h refer to the lengths of a axis and c axis in the hexagonal system, respectively, and a_r and α_r refer to the length of a axis and rhombohedral angle of $La_{1-x}Sr_xCoO_3$ in the rhombohedral system, respectively. The rhombohedral lattice parameters of the sample with x = 0.0 in this study were in good agreement with those of undoped $LaCoO_3$ at 293 K (a_r = 5.3778(1) Å and α_r = 60.798(1)°) determined by neutron diffraction (10). The cooling rate in firing sparingly affected these lattice parameters, which is in agreement with the results shown in Fig. 1. The α_r value decreased almost linearly with x and became 60° at x = 0.55 (Fig. 4d), which shows that the phase changed from rhombohedral to cubic at x = 0.55. The observed linear dependency of α_r on x shows that rhombohedral distortion is reduced by Sr-doping; hence, a_h, c_h, and a_r are expected to change monotonously with a change in x. As shown in Figs. 4a–4c, however, these lattice parameters showed anomalous behavior in the range $0.2 < x < 0.4$; a_h decreased abruptly and the increase in c_h and a_r were suppressed in this region.

Figure 5 shows the structure of $R\bar{3}c$ $La_{1-x}Sr_xCoO_3$ based on a simple cubic unit cell. Only oxygen atoms (6e site) can change their position in the $R\bar{3}c$ space group; the other atoms are fixed at the equivalent positions (La or Sr; 2a site, Co; 2b site). All Co–O distances and Co–O–Co angles in Fig. 5 are equal, whereas there are three kinds of La–O distance because of the tilting of adjacent CoO_6 octahedra along the cubic axis. The La–O distances, Co–O distance, and Co–O–Co angle were calculated from the optimized fitting parameters and are plotted against x in Fig. 6. For the sample with $x = 0.0$, the values were in good agreement with the data reported for undoped $LaCoO_3$ at 293 K (d_{La-O} = 2.451, 2.702, and 2.992 Å, d_{Co-O} = 1.932 Å, and Co–O–Co angle = 163.91°) determined by neutron diffraction (10). The three La–O distances gradually came closer to one another with an increase in x and became equal in length at $x = 0.55$ (Fig. 6a) because of the phase transition from rhombohedral to cubic. After a slight increase at $x < 0.1$, the Co–O distance decreased with x in the range $0.1 < x < 0.5$ and changed abruptly at $x = 0.55$ due to the phase transition (Fig. 6b). The Co–O–Co angle increased slightly at $x < 0.5$ and changed abruptly to 180° at $x = 0.55$ (Fig. 6c).

Closer examination of these parameters in the rhombohedral region ($0.0 \le x \le 0.5$) in Fig. 6 reveals that in all cases the changes in the range $0.25 < x < 0.3$ were more drastic than those in the other range; the three La–O distances came closer to one another, the Co–O distance showed an abrupt decrease, and the Co–O–Co angle increased abruptly in the range $0.25 < x < 0.3$. The abrupt decrease in the Co–O distance caused lattice contraction and was responsible for the anomalous behavior of lattice parameters observed in the range $0.2 < x < 0.4$ in Fig. 4. It should be noted that no change in lattice symmetry was observed in this range. The abrupt changes observed in Fig. 6, in particular, the Co–O distance and Co–O–Co angle, are considered to be closely related to the electric properties of $La_{1-x}Sr_xCoO_3$, and this correlation is discussed in the following sections.

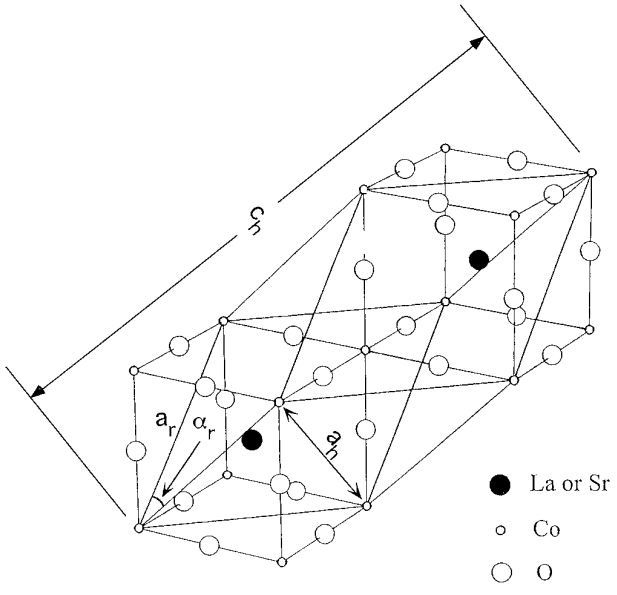

FIG. 3. The cubic and rhombohedral unit cells of $La_{1-x}Sr_xCoO_3$ in the cubic region ($0.55 \le x \le 0.7$). The rhombohedral and hexagonal lattice parameters are indicated in the figure. In the rhombohedral region ($0.0 \le x \le 0.5$), α_r increases from 60°, and a_h and c_h show an increase and decrease with x, respectively.

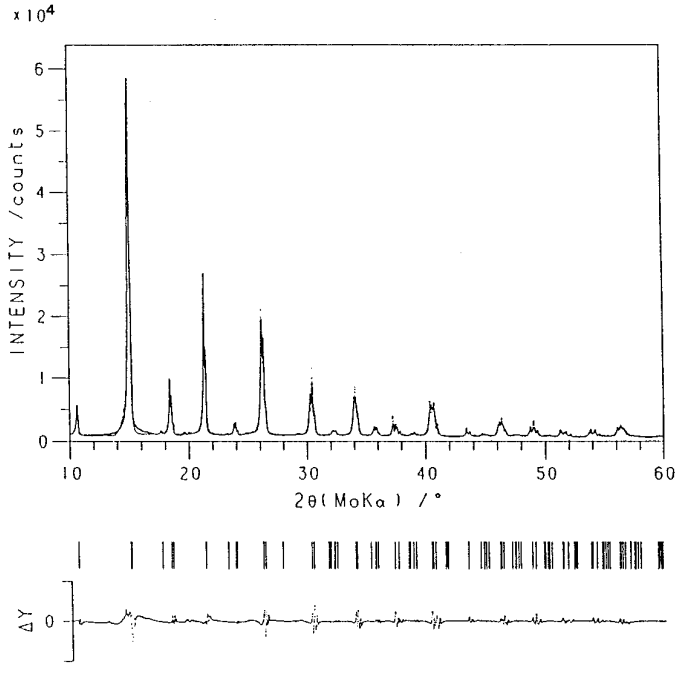

FIG. 2. Rietveld refinement plot for fast-cooled $La_{0.7}Sr_{0.3}CoO_3$. The calculated and observed patterns are shown by solid line and dots, respectively. The vertical marks show the positions of calculated reflections. The trace in the bottom is a plot of the differences between the observed and calculated intensities. R_{wp} is 7.7%.

3.3 *Electrical Conductivity*

The temperature dependences of conductivity (σ) of the system $La_{1-x}Sr_xCoO_3$ are shown in Fig. 7. The conductivity of the samples with $x < 0.25$ showed semiconductive behavior in the vicinity of room temperature; that is, it increased with temperature. When temperature was raised further, σ showed a maximum and decreased with temperature; that is, the conductive mechanism changed from semiconducting to metallic. The conductivity at room temperature increased with an increase in x for the samples with $x < 0.25$. This increase is attributed to an increase in the concentration of the charge carrier, hole, by Sr-doping as indicated by iodometry. The M–I transition of $La_{1-x}Sr_x$

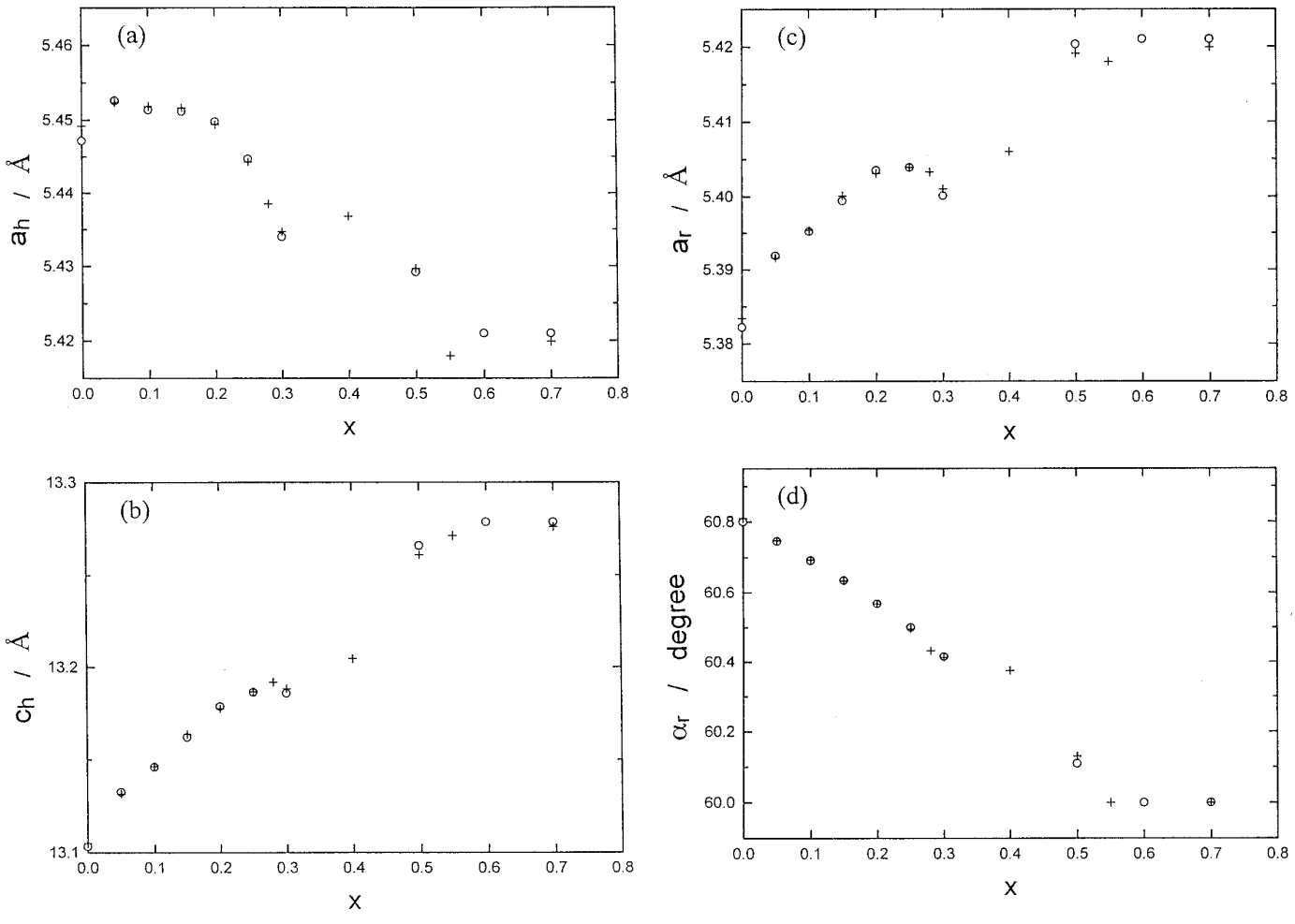

FIG. 4. Variation of (a) *a*-axis length, a_h, (b) *c*-axis length, c_h, in the hexagonal system, (c) *a*-axis length, a_r, and (d) rhombohedral angle, α_r, in the rhombohedral system of $La_{1-x}Sr_xCoO_3$; (○) cooled at ca. 873 K/h, and (+) cooled at 42 K/h after annealed at 1273 K for 12 h. Standard deviations are much smaller than the sizes of the symbols.

CoO_3 at room temperature occurred at $x \sim 0.25$, because σ of the samples in the range $0.25 < x \leq 0.7$ showed metallic behavior even at room temperature. It should be noted that the abrupt changes in Co–O distance and Co–O–Co angle in Fig. 6 were observed in the same region of x.

Mizusaki *et al.* (12) measured the electric conductivity of $La_{1-x}Sr_xCoO_3$ under 1 atm O_2 atmosphere. They observed the M–I transition at room temperature in the range $0.3 < x < 0.5$, which was slightly higher than that observed in this study. Since the conductivity was measured in air in this study, our samples would have contained more oxygen vacancies than those of Mizusaki *et al.*, the presence of which was confirmed by iodometry. Hence oxygen nonstoichiometry may play an important role in M–I transition as Sr concentration and temperature also do.

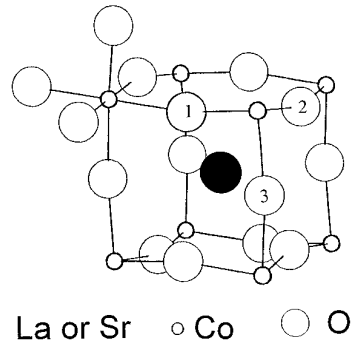

FIG. 5. "Distorted" cubic structure of $La_{1-x}Sr_xCoO_3$ perovskite. All Co–O distances and Co–O–Co angles are equal. Three kinds of La–O distances exist because of the displacement of oxygen atoms (1, 2, and 3).

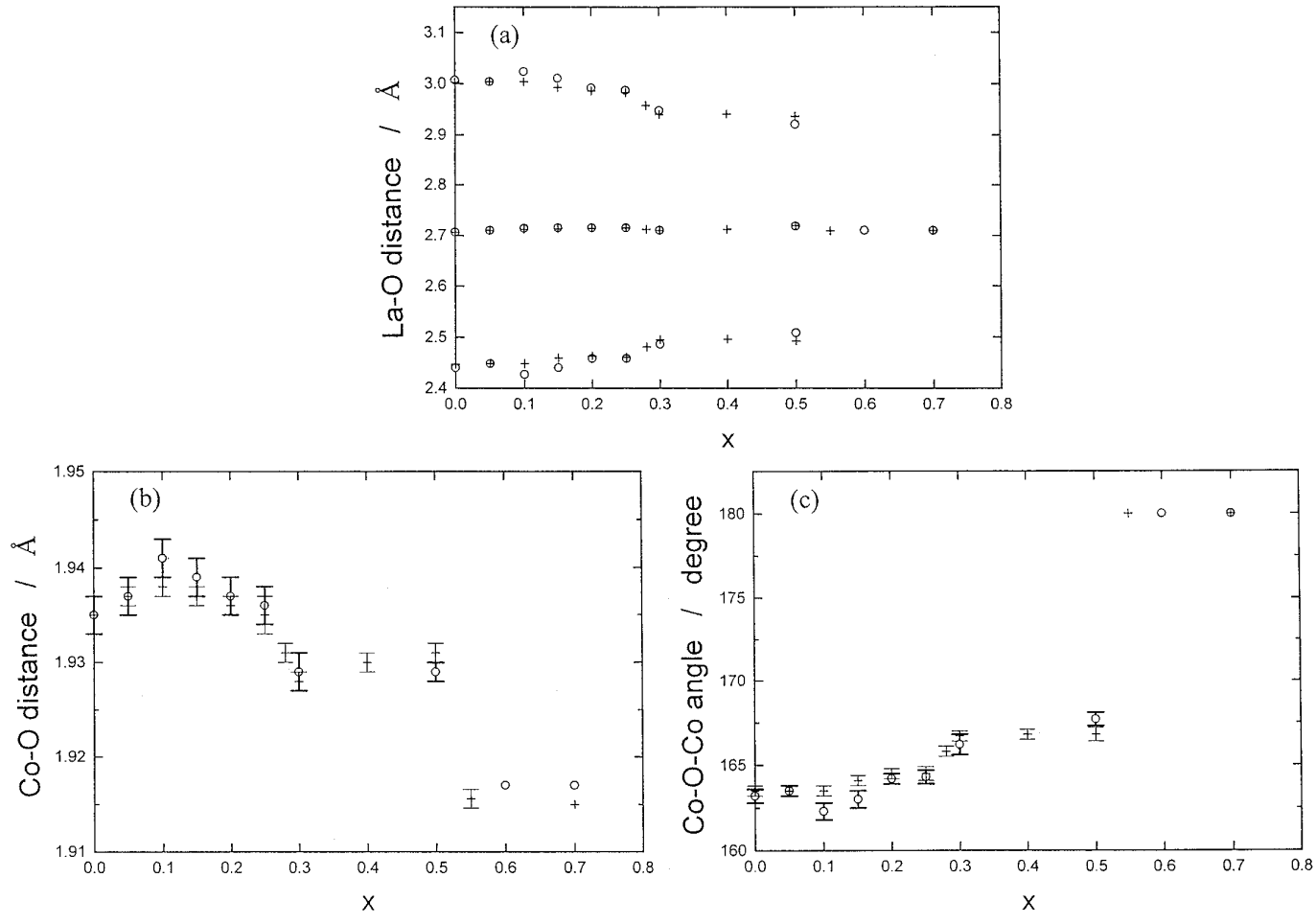

FIG. 6. Interatomic distances and angle plotted as a function of x; (a) La–O distance, (b) Co–O distance, and (c) Co–O–Co angle.

3.4 Correlation between the Crystal Structure and M–I Transition of $La_{1-x}Sr_xCoO_3$

The conduction mechanism of $La_{1-x}Sr_xCoO_3$ has been discussed for several decades (4, 6–8, 11). Since d–d Coulomb repulsion energy disturbs the motion of electrons (electron correlation effects), many transition-metal oxides behave as insulators (or semiconductors), although they are expected to be metallic based on the band theory. The M–I transition of $LaCoO_3$ has been attributed to an overlap of the Co-3d-derived t_{2g} level with the 3d-derived e_g band by Goodenough (6–8). However, the description of the M–I transition in $LaCoO_3$ has not been satisfactorily explained, being described only in terms of the electronic structure of cobalt.

Recently, Zaanen, Sawatzky, and Allen (ZSA) (24) summarized the band gaps and electronic structures of transition-metal compounds in a diagram and proposed a theory for the M–I transition. Figure 8 shows a schematic electronic structure for transition-metal oxides (13). According to the ZSA framework, insulating (as well as semiconducting) transition-metal compounds are classified into two groups. The first group is a Mott–Hubbard insulator shown in Fig. 8b. Because of the Mott–Hubbard splitting (U), the d-bands of transition metal are separated into upper and lower Hubbard bands, which creates a band gap between the two Hubbard bands. The other group is a charge-transfer (CT) insulator (25) shown in Fig. 8d), which has an energy difference (Δ) as a band gap between the p-bands of ligand anions and an upper Hubbard band of transition metal. Metallic conductivity will be attained if either of these two gaps (U or Δ) becomes smaller than bandwidth (W) as shown in Figs. 8a and 8e. Over the past few years, Sarma *et al.* (26, 27) proposed that it should be necessary to modify the ZSA diagram for transition-metal oxides that have strong covalent bonds and to include a third category of insulators, that is, a covalent insulator. In this regime, the compounds are characterized by strong covalency effects and have a large U and a small or negative Δ values, being located in a low Δ metal (Fig. 8e) if they

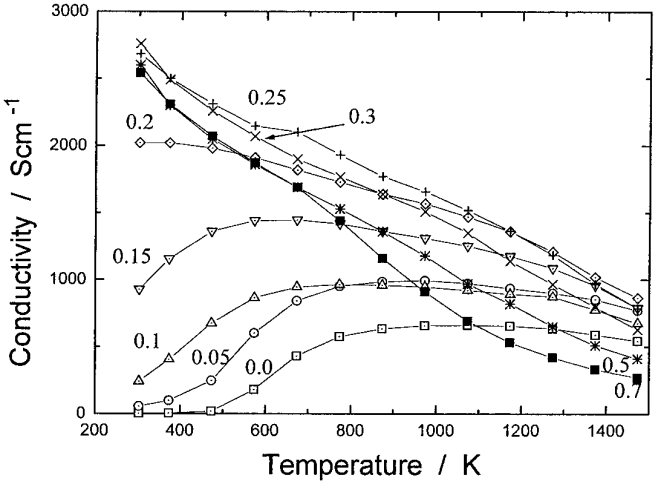

FIG. 7. Temperature dependencies of electrical conductivity of fast-cooled $La_{1-x}Sr_xCoO_3$ ($0.0 \leq x \leq 0.7$) samples measured by d.c. four-probe method in air.

have no covelant bonds. Owing to sizable coavalency effects, the covalent insulator has a similar electronic structure as a CT insulator (26) while it is expected to have metallic behavior from the values of U and Δ in the ZSA framework. Torrance *et al.* (13) calculated the values of U and Δ for many transition-metal oxides using a simple ionic model and explained the reason why these oxides show metallic or insulating behavior. They showed that $LaCoO_3$ is a CT insulator, and this was later confirmed by a soft-X-ray absorption study (14) and optical reflectivity spectroscopy (15).

In the present crystallographic study of $La_{1-x}Sr_xCoO_3$, the Co–O distance and Co–O–Co angle changed abruptly at $x \sim 0.25$ as shown in Figs. 6b and 6c, where the M–I transition at room temperature occurred as shown in Fig. 7. Hence, it is expected that there is a correlation between these anomalies and the M–I transition. Torrance *et al.* (28) reported that lattice contraction occurs at a temperature of the M–I transition of $RNiO_3$ (R = Pr, Nd, Sm) CT insulator, or it may be well described as a covalent insulator in the modified-ZSA diagram (29). They inferred that the M–I transition is most probably caused by the closing of the CT gap, which is located between the occupied O-2*p* valence band and the unoccupied Ni-3*d* conduction band, due to an increase in the electronic bandwidth with temperature. The M–I transition in $La_{1-x}Sr_xCoO_3$ system with increasing x is considered to be caused in a manner similar to that of $RNiO_3$, that is, by an increase in the electronic bandwidth, although the effects arising from doping of charge carriers are not described in the ZSA framework. Replacing La^{3+} with Sr^{2+} induces doped states within the band gap (Δ) of the $LaCoO_3$ CT insulator and the states broaden into a band with increasing x, overlapping with the valence band at M–I transition (14). The increase in electronic bandwidth and the enhancement of the overlap

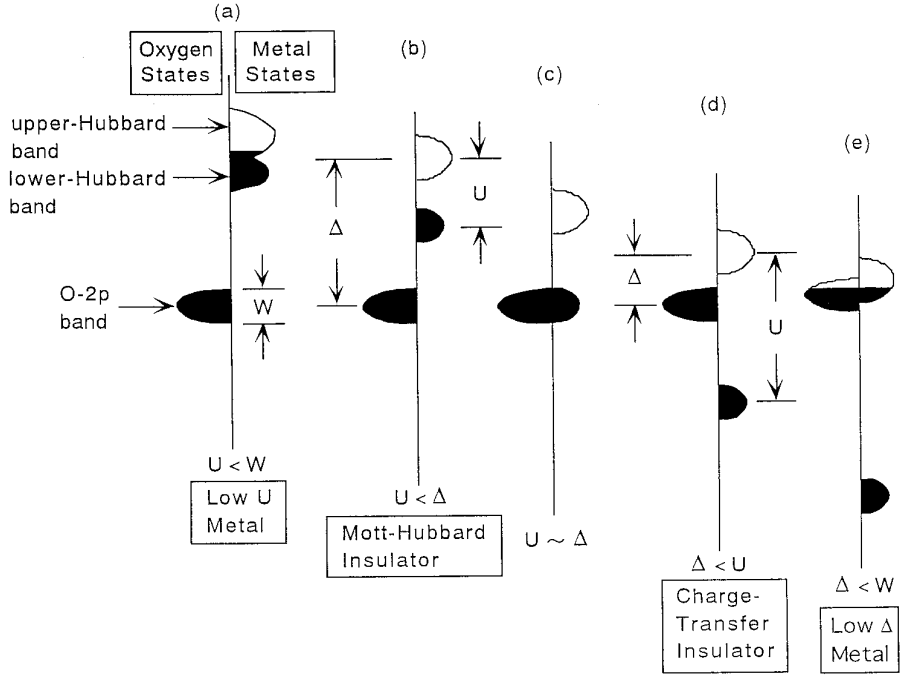

FIG. 8. Schematic diagrams for the electronic structure of transition metal oxides. U, Δ, and W denotes the Mott–Hubbard splitting, charge transfer energy, and bandwidth, respectively.

between the valence band and doped states at the M–I transition lead to a decrease in the Co–O bond length and an increase in the Co–O–Co angle. It is therefore concluded that the abrupt changes found in the present work were caused by a change in the electronic band structure at the M–I transition, that is, an increase in the overlap between the valence band and doped states.

4. CONCLUSIONS

The crystal structure of $La_{1-x}Sr_xCoO_3$ ($0.0 \leq x \leq 0.7$) was precisely determined by a powder X-ray Rietveld method. At around $x = 0.25$ the Co–O distance and Co–O–Co angle of this system showed an abrupt decrease and increase, respectively, and conductivity behavior changed from semiconducting to metallic. These abrupt changes found in the present crystallographic work were caused by a change in the electronic band structure at the M–I transition, that is, an increase in the overlap between the valence band and doped states.

ACKNOWLEDGMENTS

Computation time for Rietveld refinements was provided by the Supercomputer Laboratory, Institute for Chemical Research, Kyoto University. This work was supported by Grant-in-Aids for Scientific Research 06650779 and 07239105 from the Ministry of Education, Science and Culture, Japan.

REFERENCES

1. C. S. Tedmon Jr., H. S. Spacil, and S. P. Mitoff, *J. Electrochem. Soc.* **116,** 1170 (1969).
2. Y. Kaga, Y. Ohno, K. Tsukamoto, F. Uchiyama, M. J. Lain, and T. Nakajima, *Solid State Ionics* **40/41,** 1000 (1990).
3. Y. Teraoka, H. Zhang, S. Furukawa, and N. Yamazoe, *Chem. Lett.* 1743 (1985).
4. G. H. Jonker and J. H. Van Santen, *Physica* **19,** 120 (1953).
5. W. C. Koehler and E. O. Wollan, *J. Phys. Chem. Solids* **2,** 100 (1957).
6. J. B. Goodenough, *J. Phys. Chem. Solids* **6,** 287 (1958).
7. P. M. Raccah and J. B. Goodenough, *Phys. Rev.* **155,** 932 (1967).
8. P. M. Raccah and J. B. Goodenough, *J. Appl. Phys.* **39,** 1209 (1968).
9. V. G. Bhide, D. S. Rajoria, C. N. R. Rao, G. Rama Rao, and V. G. Jadhao, *Phys. Rev. B* **12,** 2832 (1975).
10. G. Thornton, B. C. Tofield, and A. W. Hewat, *J. Solid State Chem.* **61,** 301 (1986).
11. G. Thornton, F. C. Morrison, S. Partington, B. C. Tofield, and D. E. Williams, *J. Phys. C.* **21,** 2871 (1988).
12. J. Mizusaki, J. Tabuchi, T. Matsuura, S. Yamauchi, and K. Fueki, *J. Electrochem. Soc.* **136,** 2082 (1989).
13. J. B. Torrance, P. Lacorre, C. Asavaroengchai, and R. M. Metzger, *Physica C* **182,** 351 (1991).
14. D. D. Sarma, A. Chainani, R. Cimino, P. Sen, C. Carbone, M. Mathew, and W. Gudat, *Europhys. Lett.* **19,** 513 (1992).
15. T. Arima, Y. Tokura, and J. B. Torrance, *Phys. Rev. B* **48,** 17006 (1993).
16. A. Chainani, M. Mathew, and D. D. Sarma, *Phys. Rev. B* **46,** 9976 (1992).
17. H. Eisaki, T. Ido, K. Magoshi, M. Mochizuki, H. Yamatsu, T. Ito, and S. Uchida, *Physica C* **185–189,** 1295 (1991).
18. T. Yao, Report of Grand-in-Aid for Scientific Research 02650560 from the Ministry of Education, Science and Culture, Japan, 1992, p. 34.
19. Y. Oka, T. Yao, and N. Yamamoto, *J. Solid State Chem.* **86,** 116 (1990).
20. T. Yao, Y. Oka, and N. Yamamoto, *Mater. Res. Bull.* **27,** 669 (1992).
21. Y. Oka, T. Yao, N. Yamamoto, Y. Ueda, and A. Hayashi, *J. Solid State Chem.* **105,** 271 (1993).
22. T. Yao, Y. Oka, and N. Yamamoto, *J. Solid State Chem.* **122,** 196 (1994).
23. T. Ishigaki, S. Yamauchi, K. Kishio, J. Mizusaki, and F. Fueki, *J. Solid State Chem.* **73,** 179 (1988).
24. J. Zaanen, G. A. Sawatzky, and J. W. Allen, *Phys. Rev. Lett.* **55,** 418 (1985).
25. S. Hüfner, *Solid State Commun.* **49,** 1177 (1984).
26. D. D. Sarma, *J. Solid State Chem.* **88,** 45 (1990).
27. S. Nimkar, D. D. Sarma, H. R. Krishnamurthy, and S. Ramasesha, *Phys. Rev. B* **48,** 7355 (1993).
28. J. B. Torrance, P. Lacorre, A. I. Nazzal, E. J. Ansaldo, and Ch. Niedermayer, *Phys. Rev. B* **45,** 8209 (1992).
29. S. R. Barman, A. Chainani, and D. D. Sarma, *Phys. Rev. B* **49,** 8475 (1994).